DOI: 10.17344/acsi.2018.4376 *Acta Chim. Slov.* **2019,** *66,* 542–551

Scientific paper

Synthesis and Study of Catalytic, Anti–Bacterial, Anti–Oxidant, and DNA Cleavage Properties of Ag–Co and Ag–Ni Magnetic Nanoparticles

Keveh Pravanak Boroujeni,[1,*] Mansooreh Shahrokh,[1] Jamshid Karvani,[1] Niloofar Moradi,[1] Ahmad Farokhnia[1] and Mohsen Mobini[2]

[1] *Department of Chemistry, Shahrekord University, Shahrekord (115), Iran*

[2] *Department of Genetics, Shahrekord University, Shahrekord (115), Iran*

* *Corresponding author: E-mail: parvanak-ka@sci.sku.ac.ir*
Tel.: +0098-38-32324401; fax: 0098-38-32324419

Received: 03-06-2018

Dedicated to the memory of Mrs Zohreh Hoseini

Abstract

Magnetic Ag–Co and Ag–Ni alloy nanoparticles were prepared through a chemical reduction method using their corresponding $[Co(NH_3)_6]Cl_3$ and $[Ni(C_2O_4)_2]K_2$ complexes, and $AgNO_3$. In this reaction, hydrazine monohydrate was used as reducing agent. The obtained nanoparticles were characterized by Fourier transform infrared spectroscopy (FT-IR), scanning electron microscopy (SEM), energy dispersive spectroscopy (EDS), X-ray diffraction (XRD), and vibrating sample magnetometer (VSM). Ag–Co and Ag–Ni nanoalloys exhibited excellent catalytic performance in the preparation of 1,8–dioxooctahydroxanthenes from the reaction of 5,5-dimethyl-1,3-cycloheanedione (dimedone) with aromatic aldehydes. Catalysts were separated by an external permanent magnet and reused. Both, Ag–Co and Ag–Ni nanoalloys posess antibacterial and antioxidant properties and have no significant effect on DNA cleavage.

Keywords: Nanoalloys; magnetism and magnetic properties; 1,8–dioxooctahydroxanthenes; anti-bacterial activity; anti-oxidant activity; DNA cleavage properties

1. Introduction

Binary or multi-metal alloys have attracted growing research interest in recent years in both industrial and laboratory chemical processes due to their unique and novel optical, electrical, and catalytic properties.[1–4] Alloying two or more metals can improve the mechanical, chemical, electrical, and thermal conductivity properties of pure metals.[5] Among metallic alloys, nanoalloys are gaining increasing importance and have several advantages over their corresponding bulk forms. For example, the Ag–Ni alloy is immiscible in bulk form, and have no tendency to form any solid solution.[6] Further, the bulk form of Ag–Co has large miscibility gaps,[7] whereas both Ag–Ni and Ag–Co nanoalloys show good solid solubility properties.[8,9]

Among multiple nanoalloys, silver nanoalloys have many specific properties that make them very attractive and valuable in biomedical areas, catalysis, and magnetic imaging purposes.[10] For instance, Ag–Ni nanoalloys have strong anti-oxidation properties[11] and have been used in the electrocatalytic reduction of benzyl chloride.[12] Also, Ag–Co nanoalloys have the ability to catalyze the oxygen reduction reactions[13] and have been used in catalytic oxidation of formaldehyde.[14]

Xanthene derivatives containing reactive pyran ring system are particularly attractive because of their biological and therapeutic properties such as anti-inflammatory,[15] anti-depressant,[16] and anticancer activities.[17] Xanthene-dye-labelled phosphatidylethanolamines have been used as probes for fluorescence-ratio measurements of interfacial pH in cellular systems.[18] Also, xanthenes have been shown to be efficient laser dyes with high photostability.[19] 1,8-Dioxooctahydroxanthenes are one of the most important derivatives of xanthenes. A convenient method for the synthesis of 1,8-dioxooctahydroxanthenes is reac-

tion between an aldehyde (1 equiv) and dimedone (2 equiv) in the presence of a catalyst such as *p*-dodecylbenezenesulfonic acid,[20] Amberlyst-15,[21] $SmCl_3$,[22] carboxy functionalized ionic liquid,[23] $SiCl_4$,[24] ceric ammonium nitrate (CAN),[25] $[Et_3NH][HSO_4]$,[26] CAN-supported HY-zeolite,[27] piperidine/HCl,[28] Mg–Al hydrotalcite,[29] thiourea dioxide,[30] hydroxylamine-*O*-sulfonic acid,[31] carbon nanotube-$BuSO_3H$,[32] cellulose/Al_2O_3-[MeIm]Cl-$XAlCl_3$,[33] sulfated zirconia,[34] and L-pyrrolidine-2-carboxylic acid sulfate (LPCAS).[35] Most of these catalysts, however, have numerous disadvantages such as waste production, corrosion problems, no catalyst recovery, low yields, high reaction temperature, long reaction times, tedious work-up, and the formation of the uncyclized product 2,2'-aryl-methylenebis(3-hydroxy-2-cyclohexene-1-one) derivatives. Thus, it is an exciting challenge to find new catalysts with high activity and selectivity.

One of the most important strategies for magnetic nanoalloys synthesis is a reduction method, and one of the most useful agents for this reaction is hydrazine monohydrate.[36] During the reduction process, if primary elements have different reduction properties they will form a core shell structure, otherwise this reaction will lead to a bimetallic nanoalloy generation.[37] Along this line and in continuation of our ongoing research on the synthesis and applications of nanocatalysts and nanoalloys,[38,39] we were prompted to explore the efficacy of Ag–Co and Ag–Ni magnetic nanoalloys as heterogeneous catalysts for the synthesis of 1,8-dioxooctahydroxanthenes. Also, the biological activities of these nanoalloys were studied.

2. Experimental

2. 1. Materials and Methods

Commercially available reagent grade chemicals were used as received. Two bacterial strains were used: *E.coli* (ATCC 35218) and *S.aureus* (ATCC 6538). XRD patterns were recorded by a Phillips, X–ray diffractometer using graphite monochromatized Cu Kα radiation. Scanning electron microscopy (SEM) images were taken with a MIRA3 FEG-SEM, and energy-dispersive spectroscopy (EDS) analysis was studied by LEO 1455 VP microscope. Room temperature magnetic properties were investigated by Lakeshore device in an applied magnetic field sweeping between ±10000 Oe. Reaction monitoring and purity determination of the products were accomplished by GLC or TLC on silica-gel polygram SILG/UV254 plates. Gas chromatography was recorded on Shimadzu GC 14–A. IR spectra were obtained by a Shimadzu model 8300 FT–IR spectrophotometer. ^{1}H NMR spectra were recorded on 400 MHz spectrometer in $CDCl_3$. Melting points were determined on a Fisher–Jones melting–point apparatus.

2. 2. Synthesis of Ag–M (M = Ni, Co) Nanoalloys

$[Ni(C_2O_4)_2]K_2$ and $[Co(NH_3)_6]Cl_3$ complexes were synthesized using as described in the literature, respectivly.[40,41] In a typical procedure, 0.5 g (1.60 mmol) of $[Ni(C_2O_4)_2]K_2$ complex was dissolved in 25 mL of a mixture of water–ethanol (50:50). Then, a solution of $AgNO_3$ (25 mL, 0.064 M) was gradually added to the above solution. After that, 5 mL of hydrazine (excess) and 5 mL of NaOH (4 M) were added to above mixture at 70–80 °C and the resulting mixture was stirred at this temperature. As the reduction reaction proceeded, the solution turned to black after 1 h. The Ag–Ni nanoalloys were carefully decanted and washed repeatedly with doubly distilled water. Then, the product was dried at room temperature for 24 h.

The Ag–Co nanoalloys were synthesized in similar method with 0.5 g (1.87 mmol) of $[Co(NH_3)_6]Cl_3$ complex and 25 mL of $AgNO_3$ (0.075 M).

2. 3. Typical Procedure for the Preparation of 1,8-Dioxooctahydroxanthene Using Ag–Ni and Ag–Co Nanoalloys

To a solution of 3-nitrobenzaldehyde (1 mmol, 0.15 g), dimedone (2 mmol, 0.28 g) and ethanol (3 mL) in a round-bottom flask, Ag–Ni (0.06 g) or Ag–Co nanoalloys (0.05 g) was added. The reaction mixture was magnetically stirred at room temperature. Progress of the reaction was monitored by TLC and GC. After completion of the reaction, the catalyst was removed by an external magnet and washed with ethanol (2 × 10 mL). Then, the filtrate was concentrated on a rotary evaporator under reduced pressure and the crude product recrystallized from ethanol to afford the pure product 3,4,6,7-tetrahydro-3,3,6,6-tetramethyl-9-(3-nitrophenyl)-2H-xanthene-1,8(5H,9H)-dione. ^{1}H NMR (400 MHz, $CDCl_3$) δ = 1.02 (6H, *s*, $2CH_3$), 1.14 (6H, *s*, $2CH_3$), 2.17–2.29 (4H, *m*, $2CH_2$), 2.53 (4H, *s*, $2CH_2$), 4.86 (1H, *s*, CH), 7.41–8.04 (4H, *m*, Ar-H).

2. 4. Antibacterial Performance of Ag–Ni and Ag–Co Nanoalloys

Disk diffusion test is performed by applying a bacterial inoculum to the surface of Muller-Hinton agar plates (100 mm diameter) using sterile swabs. First, *E.coli* and *S.aureus* cells were separately cultured from pure bacterial to nutrient broth media, and incubated at 37 °C until reaching to 0.5 McFarland standards. After incubation of plates at 37 °C for 24 h and growth of the bacterial, distinct equal wells have been created in the agar plates for antibacterial diffusion assay. Afterwards, dispersed solutions of Ag–Ni or Ag–Co nanoalloys (0.64, 0.32, 0.16 or 0.08 mg/mL) were individually poured into the wells. Plates were incubated for 18–24 h at 37 °C to determine the zone sizes of bacterial growth inhibition in millimeter

scale. Sterile distilled water and standard antibiotic discs were used as negative and positive controls, respectively.

2. 5. Free Radical Scavenging Activity of Ag–Ni and Ag–Co Nanoalloys

At first, a methanol solution of DPPH (0.1 mM) was prepared. Then, Tris–HCl buffer (450 μL, pH = 7.4) and methanolic DPPH solution (1 mL) were added to 50 μL of Ag–Ni and Ag–Co nanoalloys with distinct concentrations (2.5, 5, 10 or 20 μg/mL). The mixtures were kept at room temperature for 30 min in dark. Afterwards, the absorbance of mixtures was measured at 517 nm. The methanol was used as a blank solution. The same experiment was performed with BHT as a positive control. The DPPH free radical scavenging activity was subsequently calculated as: % DPPH radical scavenging = Control OD- sample OD/ Control OD × 100.

2. 6. DNA Cleavage Assays

Agarose gel electrophoresis was used to identify the cleavage of pET-28 plasmid DNA by Ag–Ni and Ag–Co nanoalloys. Each 40 μL of Ag–Ni or Ag–Co nanoalloys with distinct concentrations (0.25, 0.5, 1 or 2 mg/mL) were added to plasmid DNA solution (5 μL, 0.25 μg/mL) in sterile 1.5 mL micro tubes and incubated at 37 °C for 24 h. Then, the obtained mixture (10 μL) was combined with 1 μL of gel loading solution (Sigma, G2526-5ML) and loaded into the 1% agarose gel (W/V) wells. The agarose gel was prepared with TBE 1X buffer (Tris-HCl (0.07 M, pH = 7.4), EDTA (4 mL, 0.5 M, pH = 8.0), and boric acid (5.5 g)) in water (1 L). After electrophoresis (40 mA and 80 volt for 45 min), the agarose gel was observed in the gel duct device under UV rays (UVItec Limited BTS-20M).

3. Results and Discussion

3. 1. Characterization of Magnetic Ag–Co and Ag–Ni Nanoalloys

Vibration spectra (FT–IR) of Ag–Co and Ag–Ni nanoalloys are shown in Figure 1. During the chemical reactions, complete destruction of primary complexes occurs and all spherical ligand vibration disappears. Therefore, FT–IR spectra have no absorption bands in the medium IR region, just the weak absorption bands due to the water in the alloy nanoalloys are observed in the infrared spectrum.

The XRD pattern of Ag–Co and Ag–Ni nanoalloys were studied (Figure 2). Figure 2a shows that Ag–Co nanoalloys were formed of cobalt and silver phase (Figure 2a) and in this respect, cobalt reflects two structures fcc and hcp. The difference between XRD pattern of fcc and hcp cobalt is in the 2θ region 51 related to the structure of

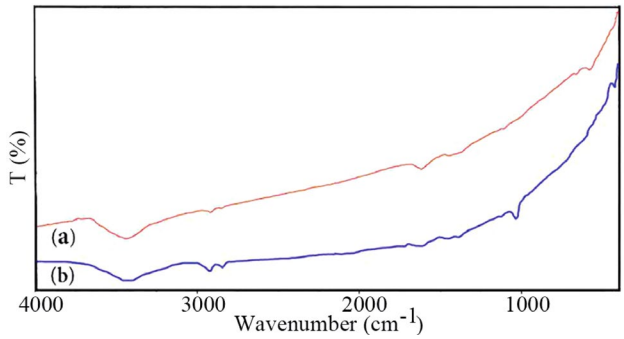

Figure 1. FT–IR spectra of (a) Ag–Co and (b) Ag–Ni nanoalloys.

fcc and 47 related to the structure of hcp (with card numbers 01-1259 and 01-1254, respectively). As shown in Figure 2a distinct diffraction peaks for structure fcc of metallic silver (with a card number 87-0717) were clearly observed at 2θ values of 38.5978, 44.7753, 64.8870 and 77.7717, corresponding to the reflections of the (111), (200), (220) and (311) crystal planes, respectively. Also, the diffraction peaks for Ag–Ni nanoalloys (Figure 2b) show that these nanoalloys are in the fcc phase. As shown in Figure 2b, this compound can be considered as Ag–Ni bimetallic nanoalloy**.** The results show that diffraction peaks were in good agreement with the standard values given nickel (with card no. 87–0712) and silver (with card no. 87–0717). In Figure 2b distinct diffraction peaks of metallic Ag are clearly observed at 2θ values of 38.3378, 44.7020, 64.6517 and 77.5765, corresponding to the reflections of the (111), (200), (220) and (311) crystal planes, respectively. In most studies of the grain size of nanocrystalline materials, X-ray line-broadening analysis is used. The crystal size of Ag–Ni and Ag–Co nanoalloys were calculated to be about 24.45 and 35.64 nm, respectively, by applying a full width at half maximum (FWHM) of the diffraction peaks and using the Debye–Scherrer equation.

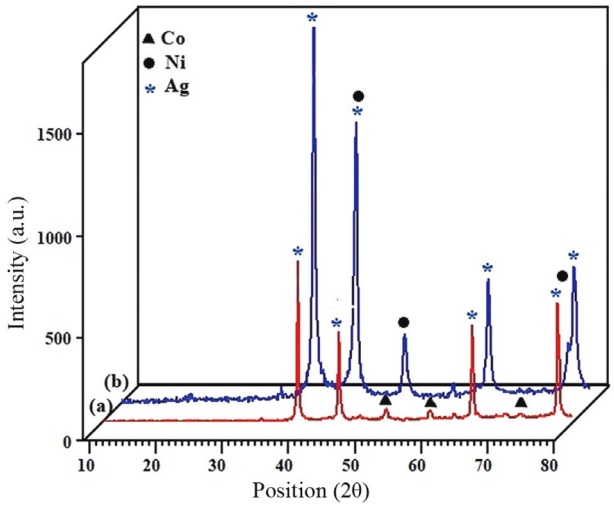

Figure 2. XRD patterns for (a) Ag–Co and (b) Ag–Ni nanoalloys.

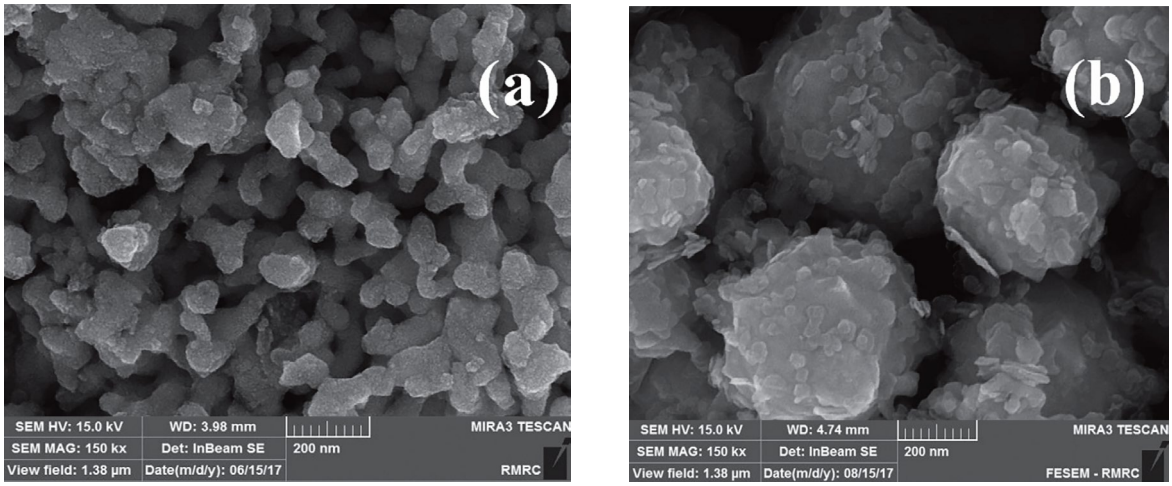

Figure 3. FE–SEM images of (a) Ag–Co and (b) Ag–Ni nanoalloys.

FE–SEM provides valuable information regarding the structural arrangement, density and geometric features of materials in the solid state. Figure 3 shows FE–SEM photographs of Ag–Co and Ag–Ni nanoalloys prepared. The FE–SEM images of Ag–Co samples (Figure 3a) show agglomerated spherical particles. The particle size distri-

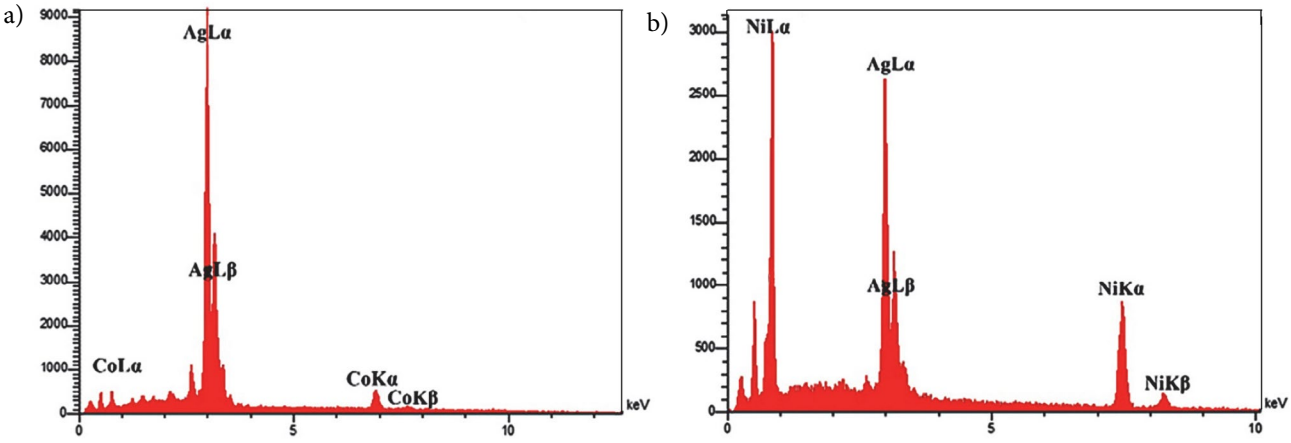

Figure 4. EDX spectra of (a) Ag–Co and (b) Ag–Ni nanoalloys.

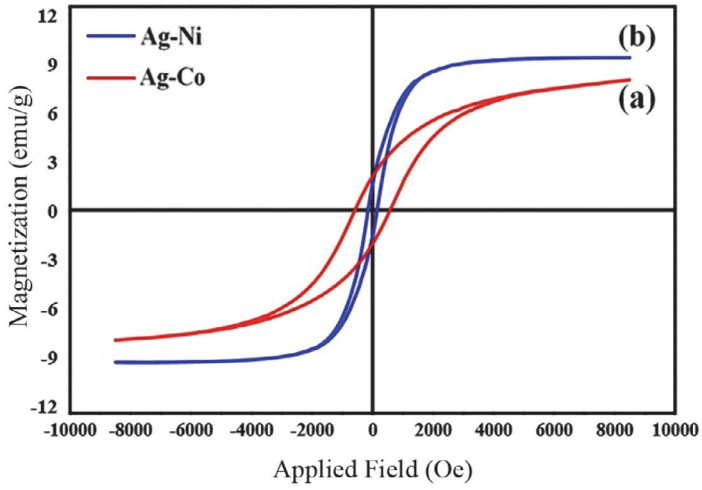

Figure 5. The magnetization curves and Ms of (a) Ag–Co and (b) Ag–Ni nanoalloys.

bution graphs for Ag–Co samples obtained from FE–SEM analysis, according to which the average diameter of a maximum number of particles is in the range of 40–50 nm. Also, the FE–SEM images show that the Ag–Ni nanoalloys have cabbage form (Figure 3b). The sizes of the nanoalloys in the lowest and maximum sizes were 26.61 and 38.23 nm, respectively.

Besides FE–SEM micrographs, the different dispersion of the phases formed using the metals can be also argued by considering energy–dispersive X–ray (EDX) data. The EDX spectra acquired at a low magnification of the powders are shown in Figure 4. EDX analysis of Ag–Co and Ag–Ni nanoalloys revealed that they are all pure bimetallic nanoalloys.

The magnetic data taken from VSM measurement of Ag–Co and Ag–Ni nanoalloys have shown in Figure 5. The hysteresis loops revealed that the resultant Ag–Co and Ag–Ni nanoalloys are ferromagnetic materials. The saturation magnetization (Ms) of Ag–Co and Ag–Ni samples (6 and 8 emu/g, at 300 K, respectively) have declined compared to Co and Ni pure nanoparticles (14 and 43 emu/g, at 300 K, respectively).[42,43] The reason for the decrease in Ms of Ag–Co and Ag–Ni samples is due to the presence of dissolved Co and Ni in the Ag matrix.

3. 2. Catalytic Applications of Ag–Co and Ag–Ni Nanoalloys

After synthesis and characterization of Ag–Co and Ag–Ni nanoalloys, we decided to investigate the efficiency of Ag–Co and Ag–Ni nanoalloys as catalysts in the synthesis of 1,8-dioxooctahydroxanthene derivatives. To optimize the amount of the catalyst, solvent and the reaction temperature, the reaction of 3-nitrobenzaldehyde (1 mmol) with dimedone (2 mmol) was studied in the various solvents and also under solvent-free conditions at different temperatures in the presence of different amounts of Ag–Co and Ag–Ni nanoalloys. The results showed that the reaction using 0.06 g of Ag–Ni nanoalloys or 0.05 g of Ag–Co nanoalloys proceeded in highest yield in ethanol at room temperature. Using lower amounts of Ag–Co and Ag–Ni nanoalloys resulted in lower yields, while higher amounts of

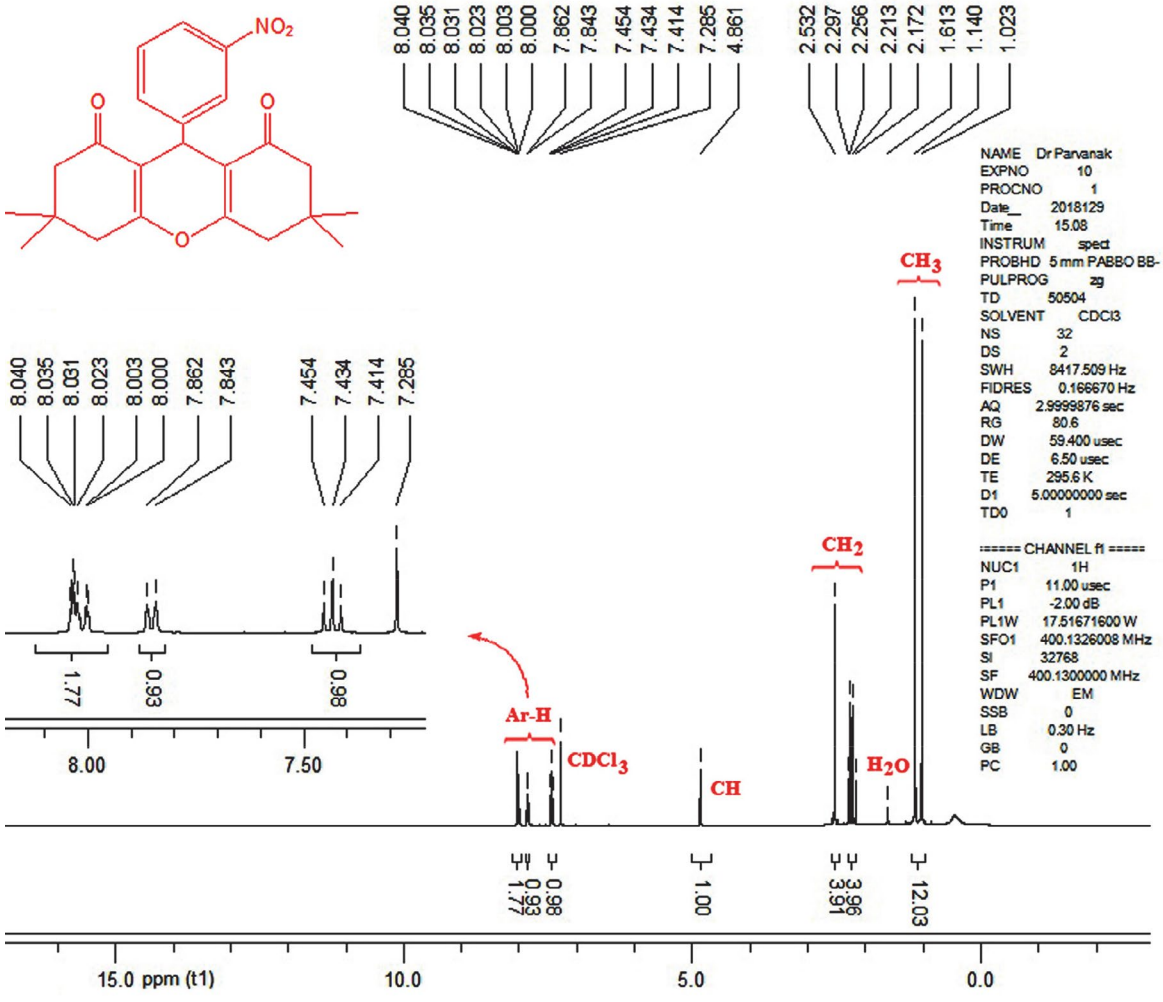

Figure 6. [1]H NMR spectrum of the 3,4,6,7-tetrahydro-3,3,6,6-tetramethyl-9-(3-nitrophenyl)-2H-xanthene-1,8(5H,9H)-dione.

Table 1: Synthesis of 1,8-dioxooctahydroxanthenes.

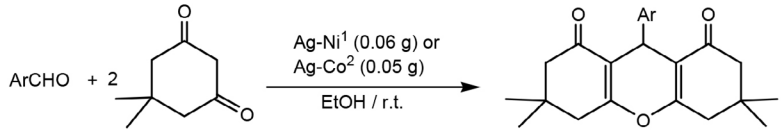

Entry	Aldehyde	Time (min)	Yield (%)[a,b]	mp (°C) (lit.)[ref.]
1	Benzaldehyde	18[1],17[2]	96[1],95[2]	200–203 (202–204)[20]
2	4-Methylbenzaldehyde	20[1],19[2]	95[1],94[2]	214–216 (217–218)[20]
3	4-Methoxybenzaldehyde	25[1],25[2]	94[1],95[2]	240–243 (242–244)[20]
4	4-Chlorobenzaldehyde	17[1],18[2]	97[1],96[2]	226–228 (228–230)[20]
5	2,4-Dichlorobenzaldehyde	16[1],17[2]	97[1],98[2]	254–255 (253–254)[20]
6	4-Hydroxybenzaldehyde	20[1],19[2]	95[1],95[2]	244–248(246–248)[20]
7	4-Bromobenzaldehyde	19[1],20[2]	96[1],97[2]	243–245 (240–242)[30]
8	4-Cyanobenzaldehyde	17[1],17[2]	97[1],96[2]	217–221 (218–220)[30]
9	4-Nitrobenzaldehyde	15[1],16[2]	97[1],97[2]	222–224 (226–228)[20]
10	3-Nitrobenzaldehyde	16[1],17[2]	96[1],98[2]	169–172 (168–170)[20]
11	1-Naphthaldehyde	21[1],22[2]	95[1],94[2]	225–226 (227–231)[33]
12	Cinnamaldehyde	27[1],24[2]	91[1],94[2]	174–176 (178–180)[26]
13	2-Thienyl carbaldehyde	21[1],23[2]	96[1],24[2]	163–165 (164–166)[23]
14	2-Furanyl carbaldehyde	20[1],22[2]	96[1],95[2]	65–67 (62–63)[29]

[a] Yields refer to the isolated pure products, [b] All the products were identified by comparing the analytical data (the spectral properties and melting points) with those reported in the literature.[20–35]

the catalysts did not affect the reaction yields and in the absence of the catalyst, nearly no product could be detected. With these results in hand, we extended our studies using different substituted benzaldehydes with both electron-withdrawing and electron-donating groups (Table 1, entries 1–10). Also, 1-naphthaldehyde and cinnamaldehyde were treated with dimedone to give the corresponding products in excellent yields (entry 11,12). Acid-sensitive aldehydes such as 2-thienyl and 2-furanyl carbaldehydes (entries 13,14) were converted to their corresponding 1,8-dioxooctahydroxanthenes without formation of any polymeric by-products. ^{1}H NMR spectrum of the 3,4,6,7-tetrahydro-3,3,6,6-tetramethyl-9-(3-nitrophenyl)-2H-xanthene-1,8(5H,9H)-dione is shown in Figure 6.

The proposed mechanism for the preparation of 1,8-dioxooctahydroxanthenes is given below in Scheme 1. The aromatic aldehyde is first activated by Ag–Co or Ag–Ni nanoalloys, which is then attacked by dimedone to yield intermediate I. Then, dehydration of intermediate I

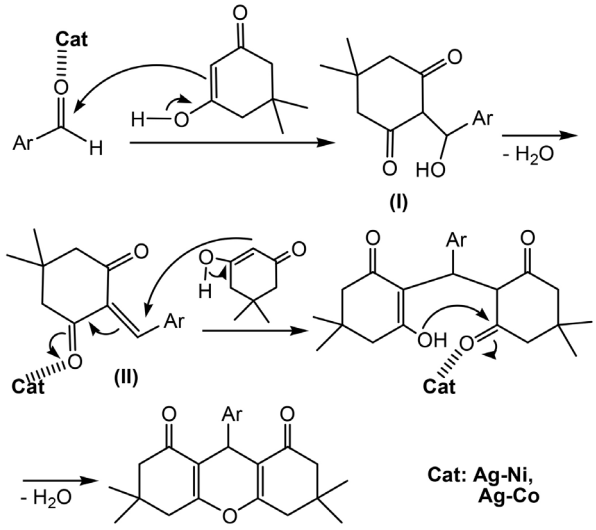

Scheme 1. The proposed mechanism for the synthesis of 1,8-dioxooctahydroxanthenes.

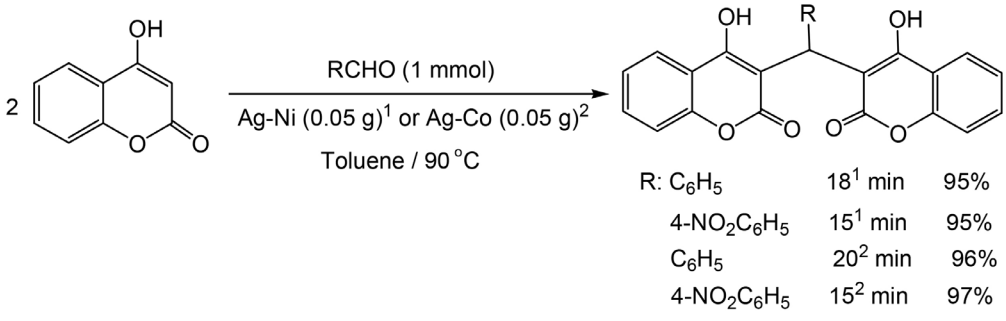

Scheme 2. Synthesis of biscoumarins in the presence of Ag–Co and Ag–Ni nanoalloys.

in the presence of nanoalloys gives the other intermediate II. Addition of a second molecule of dimedone on activated intermediate II, followed by intramolecular cyclodehydration affords the 1,8-dioxooctahydroxanthene. Based on this mechanism, it is clear that the electron withdrawing groups substituted on aromatic aldehyde in intermediate II increase the rate of nucleophilic addition of dimedone. Thus, arylaldehydes bearing the electron withdrawing groups react with dimedone faster than those containing electron releasing groups (Table 1, entries 8–10).

Following these results, we further investigated the potential of Ag–Co and Ag–Ni nanoalloys for the two component condensation of aldehydes and 4-hydroxycoumarin. As shown in Scheme 2, biscoumarins were obtained in high to excellent yields in short times.

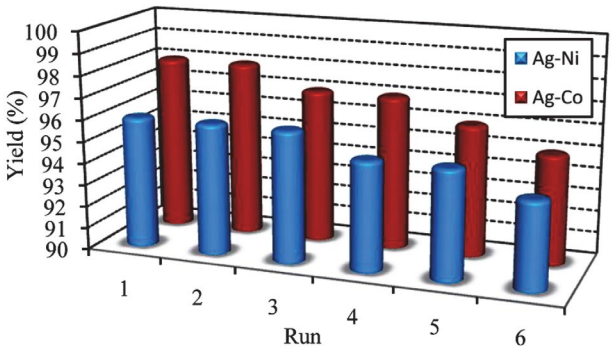

Figure 7. Recyclability of Ag–Co (0.05 g) and Ag–Ni (0.06 g) nanoalloys in the reaction of 3-nitrobenzaldehyde (1 mmol) with dimedone (2 mmol) in ethanol at room temperature after 17 and 16 min, respectively.

The reusability of the catalysts was studied. After each reaction, the catalysts were removed by an external magnet and reused for subsequent reactions with slight loss of activity (Figure 7).

By comparison of the catalytic performance of Ag–Ni and Ag–Co nanoalloys with other reported catalysts, it will be clear that these catalysts led to desired products in lower reaction times, with higher yields, at room temperature.

3. 3. Biological Activity of Ag–Co and Ag–Ni Nanoalloys

Most bacteria won't hurt humans-less than 1 percent of different types cause an infection in the human body and make people sick. Examples of bacteria that cause bacterial infections include Streptococcus, Staphylococcus, and Escherichia coli. Antibiotics are the common treatment for bacterial infections. However, numerous studies have provided strong evidence that the widespread use of antibiotics has led to the emergence of multidrug-resistant bacterial strains.[44] Despite different types of available antibiotics, few have proved effective against bacterial resistant strains. To overcome the above shortcoming of antibiotics, substantial efforts have been made by researchers constantly to introduce novel viable alternatives, for example some different types of nanoparticle-based materials with antibacterial activity. Of the range of nanoparticle options available, silver nanoparticles have received intensive interest.[45] The good performance of these nanoparticles arises from the fact that nanoparticle would be less prone to promoting resistance in bacteria than antibiotics because the mode of

Table 2: Comparison of the efficiencies of a number of different reported catalysts with that of Ag–Co and Ag–Ni nanoalloys in the reaction of benzaldehyde with dimedone.

Entry	Reaction conditions	Time (min)	Yield (%)[a]
1	*p*-Dodecylbenezenesulfonic acid, H_2O, reflux	360	89[20]
2	Amberlyst-15, CH_3CN, reflux	300	92[21]
3	$SmCl_3$, solvent-free, 120 °C	540	98[22]
4	Ionic liquid, ultrasound irradiation, r.t.	50	87[23]
5	$SiCl_4$, dichloroethane, 60–70 °C	180	90[24]
6	CAN, 2-propanol, ultrasound irradiation, 50 °C	35	98[25]
7	$[Et_3NH][HSO_4]$, solvent-free, 100 °C	20	94[26]
8	CAN supported HY-zeolite, solvent-free, 80 °C	90	88[27]
9	Piperidine/HCl, ethanol/water, r.t.	10	69[28]
10	Mg–Al hydrotalcite, H_2O, reflux	180	85[29]
11	Thiourea dioxide, H_2O, 50–60 °C	45	96[30]
12	Hydroxylamine-*O*-sulfonic acid, solvent-free, 90 °C	35	92[31]
13	Carbon nanotube-$BuSO_3H$, EtOH, r.t.	30	95[32]
14	Cellulose/Al_2O_3-[MeIm]Cl-X$AlCl_3$, EtOH, r.t.	25	91[33]
15	Sulfated zirconia, EtOH, 70 °C	480	95[34]
16	LPCAS, solvent free, 100 °C	5	95[35]
17	Ag–Co nanoalloys, EtOH, r.t	17	95
18	Ag–Ni nanoalloys, EtOH, r.t	18	96

[a]Isolated yield.

action of nanoparticles is direct contact with the bacterial cell wall, without the need to penetrate the cell.

Following the obtained results of the catalytic activity of Ag–Co and Ag–Ni nanoalloys, we try to investigate the anti-bacterial properties of these nanoalloys on viable typical microorganisms. One of the simplest tests for the evaluation of the resistance of bacteria to different materials is the disk-diffusion testing. This test is an easy, cheap and official method that is used in many clinical microbiology laboratories for antibacterial susceptibility testing. Figures 8 and 9 show the antibacterial effect of Ag–Co and Ag–Ni nanoalloys with distinct concentrations (0.64, 0.32, 0.16 or 0.08 mg/mL) on cultured microorganisms (*E.coli* and *S.aureus* cells). The results show that Ag–Co and Ag–Ni nanoalloys exhibit antibacterial properties against *E.coli* cells. In this case, Ag–Co nanoalloys have a stronger degree of bacteria growth inhibition than Ag–Ni nanoalloys. Ag–Ni nanoalloys do not show antibacterial activity against *S.aureus* cells, while Ag–Co nanoalloys have an efficient antibacterial effect on these bacteria. In each case, it is observed that the zone of growth inhibition increased with increasing the concentration of nanoalloys.

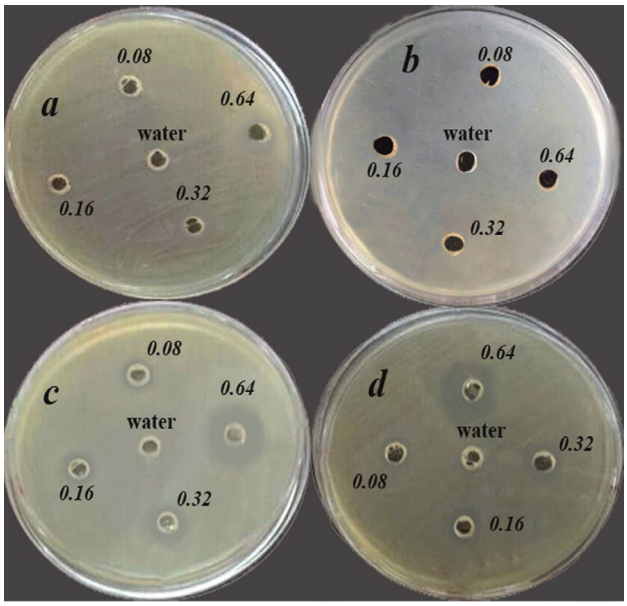

Figure 8. Evaluation of the antimicrobial activity of (a) Ag–Ni nanoalloys against *E.coli*; (b) Ag–Ni nanoalloys against *S.aureus*; (c) Ag–Co nanoalloys against *E.coli*; (d) Ag–Co nanoalloys against *S.aureus*.

Reactive oxygen species (ROS) and reactive nitrogen species (RNS) are the cellular oxidants and the free radicals which play a key role in human cancer development. Antioxidants have a defense function against carcinogens and oxidants. Recently, the estimate of antioxidant activity of nanoparticles has become one of the important basic studies in nano science.[46,47] To determine the antioxidant activity of nanoparticles, a common procedure is radical scavenging method which in 2,2-diphenyl-2-picrylhydracyl hydrate (DPPH) is used as an electron acceptor.

Encouraged by the results obtained from the antibacterial activity of Ag–Co and Ag–Ni nanoalloys, we tried to evaluate antioxidant activity of these nanoalloys with distinct concentrations (2.5, 5, 10, and 20 μg/mL) us-

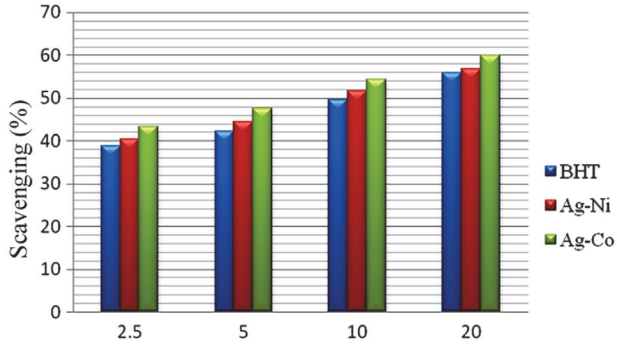

Figure 10. The DPPH radical scavenging activity of the Ag–Co and Ag–Ni nanoalloys and BHT.

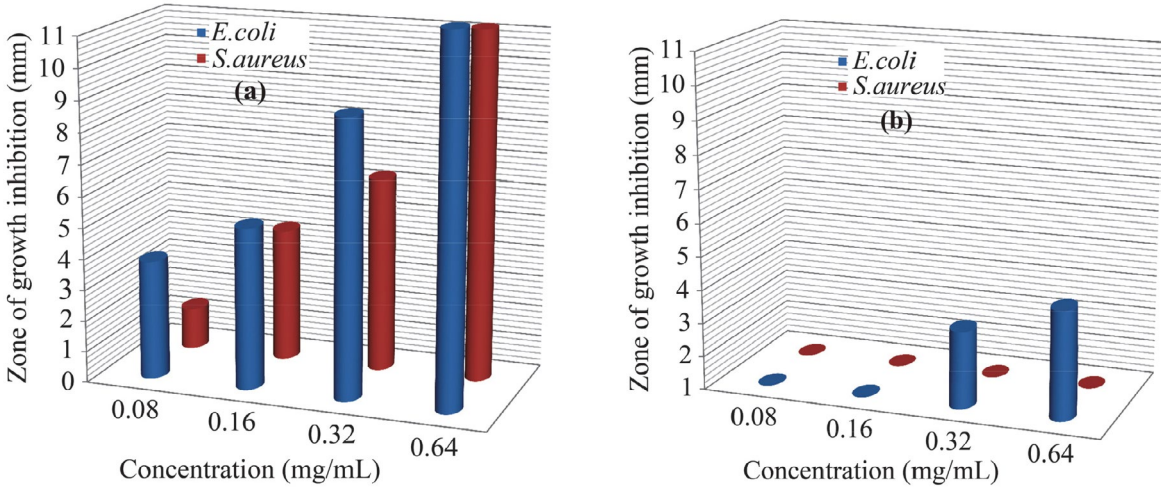

Figure 9. Antibacterial activity of (a) Ag–Co and (b) Ag–Ni nanoalloys.

Table 3: The IC_{50} values of Ag–Co and Ag–Ni nanoalloys and BHT.

Sample	IC_{50} (μg/mL)
Ag–Co nanoalloys	7.94 ± 1.48
Ag–Ni nanoalloys	11.28 ± 1.98
BHT	12.53 ± 2.43

ing butyl hydroxytoluene (BHT) as a positive control and DPPH. As the results in Figure 10 show, the following order of the antioxidant activity was observed: Ag–Co nanoalloys > Ag–Ni nanoalloys > BHT. Table 3 shows IC_{50} (the concentration of sample required to scavenge 50 % of the DPPH free radicals) value of the Ag–Co and Ag–Ni nanoalloys and BHT.

Recently, studies on the possibility of the DNA cleavage by synthetic materials such as nanoparticles have stimulated great interest.[48] Damage in DNA by free radicals is a likely reason of mutations which, if they occur in genes, may cause some of the diseases such as birth defects, genetic diseases, and cancer.[49] Following our results on antibacterial and antioxidant activities of Ag–Co and Ag–Ni nanoalloys, we decided to investigate whether or not these nanoalloys have destructive effects on DNA molecules. Based on this, we examined the effect of the distinct concentrations (0.25, 0.5, 1, and 2 mg/mL) of Ag–Co and Ag–Ni nanoalloys on the DNA cleavage. Figure 11 shows the agarose gel electrophoresis. Plasmid DNA mixed with water was used as the negative control. After exposure of plasmid DNA to different concentration of the nanomaterial suspensions, we did not observe any destructive effects on DNA molecules.

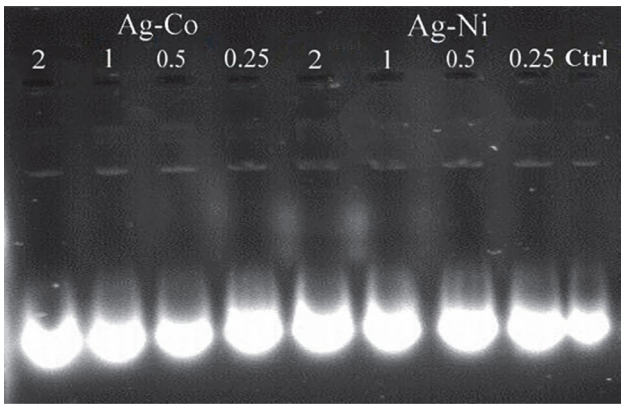

Figure 11. Effect of the distinct concentrations of Ag–Co and Ag–Ni nanoalloys on the DNA cleavage.

4. Conclusion

In summary, Ag–Co and Ag–Ni nanoalloys were easily prepared from their basic ingredients and used as highly efficient heterogeneous catalytic systems for the synthesis of 1,8-dioxooctahydroxanthene derivatives from the reaction of dimedone with aromatic aldehydes in ethanol as a green solvent at room temperature. The catalysts can be easily separated using an external magnet and their catalytic activity remains after several reaction cycles. The procedure offers several advantages including cleaner reaction profiles, simple experimental and work-up procedures, no competitive side reactions, high reaction rates, and excellent yields. To the best of our knowledge, these nanoalloys have not yet been evaluated in catalytic reactions in organic synthesis. Also, Ag–Co and Ag–Ni nanoalloys showed antibacterial and antioxidant properties and they had no destructive effects on DNA molecules.

5. Acknowledgement

We gratefully acknowledge the partial support of this study by the Shahrekord University of Technology Research Council, Iran.

6. References

1. R. Ferrando, J. Jellinek, R. L. Johnston, *Chem. Rev*. **2008***, 108*, 845–910. **DOI:**10.1021/cr040090g
2. A. Akdag, A. Tuncay Ozyilmaz, *Acta Chim. Slov.* **2017**, *64*, 312–318. **DOI:**10.17344/acsi.2016.3119
3. I. Škugor Rončević, N. Vladislavić, M. Buzuk, *Acta Chim. Slov.* **2018**, *65*, 698–708. **DOI:**10.17344/acsi.2018.4400
4. N. Bahrami Panah, I. Danaee, M. Payehghadr, A. Madahi, *Acta Chim. Slov.* **2018**, *65*, 312–318. **DOI:**10.17344/acsi.2017.3953
5. K. D. Gilroy, A. Ruditskiy, H. C. Peng, D. Qin, Y. Xia, *Chem. Rev.* **2016**, *116*, 10414–10472. **DOI:**10.1021/acs.chemrev.6b00211
6. C. Tang, L. Li, H. Gao, G. Li, X. Qiu, J. Liu, *J. Power Sources* **2009**, *188*, 397–403. **DOI:**10.1016/j.jpowsour.2008.12.011
7. T. Van Hoof, M. Hou, *Phys. Rev. B: Condens. Matter* **2005***, 72*, 115434–115446. **DOI:**10.1103/PhysRevB.72.115434
8. I. Karakaya, W. T. Thompson, *Bull. Alloy Phase Diagrams* **1988**, *9*, 237–243. **DOI:**10.1007/BF02881271
9. J. Xu, U. Herr, T. Klassen, R. S. Averback, *J. Appl. Phys*. **1996***, 79*, 3935–3945. **DOI:**10.1063/1.361820
10. J. P. Liu, E. Fullerton, O. Gutfleisch, D. J. Sellmyer (Eds.): Nanoscale Magnetic Materials and Applications, *Springer*, **2009**.
11. C. C. Lee, D. H. Chen, *Nanotechnol*. **2006***, 17*, 3094–3099. **DOI:**10.1088/0957-4484/17/13/002
12. H. H. Zhou, Y. L. Li, J. Q. Huang, C. X. Fang, S. H Dan, Y. F. Kuang, *Trans. Nonferrous Met. Soc. China* **2015***, 25*, 4001–4007. **DOI:**10.1016/S1003-6326(15)64049-3
13. A. Holewinski, J. C. Idrobo, S. Linic, *Nat. Chem*. **2014**, *6*, 828–834. **DOI:**10.1038/nchem.2032
14. Z. Qu, D. Chen, Y. Sun, Y. Wang, *Appl. Catal., A*. **2014**, *487*, 100–109. **DOI:**10.1016/j.apcata.2014.08.044
15. T. Librowski, R. Czarnecki, T. Czekaj, H. Marona, *Medicina* (*Kaunas*) **2005**, *41*, 54–58.

DOI:10.1515/hc-2017-0215
16. H. Herken, A. Gurel, S. Selek, F. Armutcu, M. E. Ozen, M. Bulut, O. Kap, M. Yumru, H. A. Savas, O. Akyol, *Arch. Med. Res*. **2007***, 38*, 247–252. **DOI:**10.1016/j.arcmed.2006.10.005
17. M. S. L. Kumar, J. Singh, S. K. Manna, S. Maji, R. Konwar, G. Panda, *Bioorg. Med. Chem. Lett*. **2018**, *28*, 778–782. **DOI:**10.1016/j.bmcl.2017.12.065
18. C. G. Knight, T. Stephens, *Biochem. J*. **1989***, 258*, 683–687. **DOI:**10.1042/bj2580683
19. M. Ahmad, T. A. King, D. K. Ko, B. H. Cha, J. Lee, *J. Phys. D: Appl. Phys*. **2002***, 35*, 1473–1476. **DOI:**10.1088/0022-3727/35/13/303
20. T. S. Jin, J. S. Zhang, J. C. Xiao, A. Q. Wang, T. S. Li, *Synlett* **2004**, *2004*, 866–870.
21. B. Das, P. Thirupathi, I. Mahender, V. S. Reddy, Y. K. Rao, *J. Mol. Catal. A: Chem*. **2006***, 247*, 233–239. **DOI:**10.1016/j.molcata.2005.11.048
22. A. Ilangovan, S. Malayappasamy, S. Muralidharan, S. Maruthamuthu, *Chem. Cent. J*. **2011***, 5*, 81–87. **DOI:**10.1186/1752-153X-5-81
23. A. N. Dadhania, V. K. Patel, D. K. Raval, *C.R. Chim*. **2012***, 15*, 378–383. **DOI:**10.1016/j.crci.2012.01.006
24. H. A. Soliman, T. A. Salama, *Chin. Chem. Lett*. **2013***, 24*, 404–406. **DOI:**10.1016/j.cclet.2013.03.021
25. N. Mulakayala, G. P. Kumar, D. Rambabu, M. Aeluri, M. B. Rao, M. Pal, *Tetrahedron Lett*. **2012***, 53*, 6923–6926. **DOI:**10.1016/j.tetlet.2012.10.024
26. Z. Zhou, X. Deng, *J. Mol. Catal. A: Chem*. **2013***, 367*, 99–102. **DOI:**10.1016/j.molcata.2012.11.002
27. P. Sivaguru, A. Lalitha, *Chin. Chem. Lett*. **2014***, 25*, 321–323. **DOI:**10.1016/j.cclet.2013.11.043
28. A. M. Reeve, *J. Chem. Educ*. **2014***, 92*, 582–585. **DOI:**10.1021/ed400457c
29. R. Gupta, S. Ladage, L. Ravishankar, *Chem. J*. **2015**, *1*, 1–4.
30. P. S. Bhale, S. B. Dongare, Y. B. Mule, *Chem. Sci. Trans*. **2015**, *4*, 246–250. **DOI:**10.7598/cst2015.969
31. M. A. Zolfigol, M. Yarie, *Org. Chem. Res*. **2016***, 2*, 1–8.
32. K. Parvanak Boroujeni, Z. Heidari, R. Khalifeh, *Acta Chim. Slov*. **2016***, 63*, 602–608. **DOI:**10.17344/acsi.2016.2291
33. K. Parvanak Boroujeni, P. Tahani, *Inorg. Nano-Met. Chem*. ***2017****, 47*, 1150–1156. **DOI:**10.1080/24701556.2017.1284103
34. S. S. Kahandal, A. S. Burange, S. R. Kale, P. Prinsen, R. Luque, R. V. Jayaram, *Catal. Commun*. ***2017****, 97*, 138–145. **DOI:**10.1016/j.catcom.2017.03.017
35. V. W. Godse, S. S. Rindhe, L. Kótai, S. R. Bembalkar, R. D. Ingle, R. P. Pawar, *Eur. Chem. Bull*. **2017***, 6*, 1–4. **DOI:**10.17628/ecb.2017.6.1-4
36. S. A. Kahani, F. Mashhadian, *J. Alloys Compd*. **2016***, 660*, 310–315. **DOI:**10.1016/j.jallcom.2015.11.070
37. M. B. Gawande, A. Goswami, T. Asefa, H. Guo, A. V. Biradar, D. L. Peng, R. Zboril, R. S. Varma, *Chem. Soc. Rev*. **2015**, *44*, 7540–7590. **DOI:**10.1039/C5CS00343A
38. K. Parvanak Boroujeni, S. Hadizadeh, S. Hasani, A. Fadavi, M. Shahrokh, *Acta Chim. Slov*. **2017***, 64*, 692–700. **DOI:**10.17344/acsi.2017.3437
39. S. A. Kahani, M. Shahrokh, *RSC Adv*. **2015**, *5*, 71601–71607. **DOI:**10.1039/C5RA09385F
40. D. P. Graddon, *J. Inorg. Nucl. Chem*. **1956***, 3*, 308–322. **DOI:**10.1016/0022-1902(56)80041-9
41. D. R. Brown, R. R. Pavlis, *J. Chem. Educ*. **1985**, *62*, 807–808. **DOI:**10.1021/ed062p807
42. H. T. Yang, Y. K. Su, C. M. Shen, T. Z. Yang, H. J. Gao, *Surf. Interface Anal*. **2004***, 36*, 155–160. **DOI:**10.1002/sia.1675
43. J. H. Hwang, V. P. Dravid, M. H. Teng, J. J. Host, B. R. Elliott, D. L. Johnson, T. O. Mason, *J. Mater. Res.* **1997**, *12*, 1076–1082. **DOI:**10.1557/JMR.1997.0150
44. L. Wang, C. Hu, L. Shao, *Int. J. Nanomed.* **2017**, *12*, 1227–1249. **DOI:**10.2147/IJN.S121956
45. D. Singh, V. Rathod, S. Ninganagouda, J. Herimath, P. Kulkarni, *J. Pharm. Res.* **2013**, *7*, 448–453. **DOI:**10.1016/j.jopr.2013.06.003
46. M. Carocho, I. C. Ferreira, *Food Chem. Toxicol*. **2013***, 51*, 15–25. **DOI:**10.1016/j.fct.2012.09.021
47. D. Das, B. C. Nath, P. Phukon, S. K. Dolui, *Colloids Surf., B* **2013***, 101*, 430–433. **DOI:**10.1016/j.colsurfb.2012.07.002
48. G. Bhabra, A. Sood, B. Fisher, L. Cartwright, M. Saunders, W. H. Evans, A. Surprenant, G. Lopez-Castejon, S. Mann, S. A. Davis, L. A. Hails, *Nat. Nanotechnol*. **2009**, *4*, 876–883. **DOI:**10.1038/nnano.2009.313
49. A. Agarwal, T. M. Said, *Hum. Reprod. Update* **2003***, 9*, 331–345. **DOI:**10.1093/humupd/dmg027

Povzetek

V prispevku je predstavljena priprava magnetnih nanodelcev zlitin Ag–Co in Ag–Ni s pomočjo kemijske redukcije z uporabo $[Co(NH_3)_6]Cl_3$ in $[Ni(C_2O_4)_2]K_2$ kompleksov ter $AgNO_3$. Kot redukcijsko sredstvo so avtorji uporabili hidrazin monohidrat. Dobljene nanodelce so karakterizirali s FT-IR spektroskopijo, SEM mikroskopijo, spektroskopijo energijske disperzije (EDS), rentgensko difrakcijo (XRD) in vibracijskim magnetometrom (VSM). Nano-zlitini Ag–Co in Ag–Ni sta pokazali odlično katalitično učinkovitost pri pripravi 1,8-dioksooktahidroksantenov v reakciji 5,5-dimetil-1,3-ciklohsandiona (dimedona) z aromatskimi aldehidi. Katalizator so po reakciji izolirali iz reakcijke zmesi s pomočjo zunanjega magneta in ga ponovno uporabili. Obe, tako Ag–Co kot Ag–Ni nano-zlitina, izkazujeta antibakterijske in antioksidativne lastnosti, hkrati pa ne vplivata na cepitev DNA.